

# A transfer-matrix Monte Carlo study of random Penrose tilings

Laurence J Shaw and Christopher L Henley†

Department of Physics, Cornell University, Ithaca, NY 14853-2501, USA

Received 6 July 1990, in final form 26 April 1991

**Abstract.** We investigate the entropic properties of a simple two-dimensional random quasicrystal model: a random tiling by the  $36^\circ$  and  $72^\circ$  rhombi. Applying the transfer matrix Monte Carlo (TMMC) method to random tilings for the first time, we have calculated the entropy as a function of phason strain. We confirm earlier results that the state of zero phason strain (i.e. ten-fold symmetry) has the largest entropy; the entropy is 0.4810 (5) per tile. In addition, by fitting the dependence of the entropy on the phason strain we determined the three stiffness constants in the phason elasticity, one of which is not measurable by previous approaches. We compare the efficacy of the TMMC method with that of other methods.

## 1. Introduction

### 1.1. Theoretical and experimental background

Since the first identification of materials with non-crystallographic long-range order in 1984 [1], extensive work has been done in the field [2-4]. Still the atomic structure and the thermodynamic mechanisms of formation are unresolved. It is not clear whether the mechanisms of formation are the same for all alloys, or whether a number of different models are needed to explain the broad range of solidification rates and varying amounts of disorder of the different families of quasicrystal forming alloys. There are currently three kinds of model: the icosahedral glass model, the perfect quasicrystal model, and the random tiling model.

Until recently, all quasicrystals were produced by thermal quenching and had a high degree of disorder [5]. Whereas the orientational correlation length was typically a micron, positional correlation lengths were on the order of a few hundred angstroms producing finite width diffraction peaks [6].

The icosahedral glass model [7, 8] is a non-equilibrium model where the system is grown from a seed icosahedron by adding icosahedra of the same orientation vertex to vertex at random locations; the positional correlation length is finite although the orientational correlation length spans the system. The positions of simulated diffraction peaks are in agreement with experiment [9]. With some annealing of a icosahedral glass growth process the peak widths will scale linearly with the phason momentum in agreement with experiment [10, 11].

† To whom correspondence should be addressed.

The perfect quasicrystal model supposes an energetic ground state with quasiperiodic long-range order [12]. Like an ideal crystal, its diffraction pattern consists solely of delta-function peaks. The existence of perfect quasicrystals as a ground state requires the unlikely microscopic characteristics of highly specific atomic bonding (in analogy to the matching rules of perfect Penrose tilings).

The random tiling model, on the other hand, supposes the system has many atomic arrangements of almost degenerate energy. The quasicrystal state is a thermal equilibrium phase (as in the perfectly quasiperiodic theory) but the role of disorder is emphasized (as in the icosahedral glass model). The phason fluctuations (see section 2) have an elastic theory of the usual gradient-squared kind. It has been shown that this implies that a random-tiling model has delta-function diffraction peaks in three dimensions [2, 13], despite the short-range phason fluctuations. There is a Debye-Waller reduction of intensity, which is transferred to diffuse scattering; these are determined quantitatively by the values of the stiffness constants. In two-dimensional systems, such as the random Penrose tiling considered in this paper, the diffraction peaks are expected to have a power-law form where the exponent in the power-law is determined by the stiffness constants. The importance of the stiffness constant has motivated our calculation, both for its direct relevance to two-dimensional quasicrystals, and as a test of our transfer-matrix method in view of possible adaptation to the three dimensional case.

In addition, it was hypothesized [13, 14] that the random tiling state might be thermodynamically stabilized because of the reduction in free energy from the configurational entropy. Models of entropically stabilized long-range order predict that the quasicrystal phase is stable at higher temperatures (less than the melting point) but a related crystal phase of slightly lower energy becomes stable at lower temperatures as the entropy term becomes less significant.

Interest in random tilings has increased since the recent discovery of equilibrium quasicrystals such as  $i(\text{AlCuFe})$  [15]. These have resolution limited diffraction peaks indicating long-range order, which is consistent with either the ideal quasicrystal model or the random-tiling model. Furthermore, some experiments have found the equilibrium quasicrystals to undergo a phase transition at lower temperatures to a periodic state [15]. This is contrary to the premises of the ideal quasiperiodic model but in agreement with predictions of the random-tiling model. Further discussion of random tilings and their relevance to experiment may be found in two brief reviews [16, 17].

Numerical studies of two- and three-dimensional random tilings confirm the existence of an entropically stabilized quasiperiodic phase [18, 19] i.e. random tilings possess long-ranged quasiperiodic order. Strandburg *et al* (1989) [19] have performed Monte Carlo simulations on the two-dimensional binary and unconstrained random tiling models. Unconstrained random tilings (see figure 1) are random tilings of  $36^\circ$  and  $72^\circ$  rhombi, i.e. Penrose rhombi. Binary random tilings are tilings of the Penrose rhombi with colouring restrictions. Binary random tilings may be mapped to disc packings, where the discs have (non-additive) radii  $\tau$  and unity. Strandburg *et al* [19] performed simulations on unconstrained random tilings of up to 3571 rhombi and estimated  $K \equiv \frac{1}{2}(K_+ + K_-) = 0.60 \pm 0.02$  and  $K_z = 0.56 \pm 0.03$ , and on binary random tilings of up to 3571 discs they estimated  $K = 0.627 \pm 0.015$ , where  $K_+$ ,  $K_-$  and  $K_z$  are the independent stiffness constants (see section 2.3). Widom *et al* [18] calculated the transfer-matrix, and thereby the tiling entropy, exactly for systems with widths of up to 13 discs. Using finite-size scaling to extrapolate to the thermodynamic limit, they estimated an entropy density per unit area of  $0.2374 \pm 0.0003$ , and  $K = 0.600 \pm 0.006$ ,

in rough agreement with Strandburg *et al.* Monte Carlo simulations of random tilings of Ammann rhombohedra [20, 21] have also confirmed the existence of long-range order in three-dimensions.

## 1.2. Plan of the paper

Here we investigate the entropic properties of unconstrained (maximally) random Penrose tilings. That is, our ensemble consists of all ways to tile the plane with rhombi of unit edge and acute angles either  $36^\circ$  or  $72^\circ$ . The number of possible tilings grows exponentially with the area of the system. Equal weight is given to each distinct configuration; in other words there is no Hamiltonian but only the tiling constraint (as in other purely entropic models such as hard spheres). It is plausible that the thermodynamic state is ten-fold symmetric, in the sense of having equal distributions of all the different possible orientations of the tiles; however, this does not necessarily imply any degree of long-range order.

To determine the long-wavelength properties, in particular the shape of diffraction peaks, it suffices to know the coarse-grained free energy (which is purely entropy in our case) in terms of the 'phason' degree of freedom. (The latter is defined in section 2.1; it will suffice to say here that ten-fold symmetry corresponds to zero phason strain and any phason strain corresponds to a deviation from this state.) Therefore, the goal of the paper is to calculate the entropy as a function of phason strain. We only consider small phason strains so this reduces to the calculation of the entropy for zero phason strain, and the stiffness constants which are coefficients of the leading terms in the expansion about this point.

Since the tiling may be decomposed into layers, a numerical transfer-matrix formulation can be used to calculate the thermodynamic properties of the tiling on a strip [14, 18, 22]. A numerically exact transfer-matrix calculation is formidable except for the narrowest strips, since the dimension of the vector space grows exponentially with the width of the system. The transfer-matrix Monte Carlo (TM-MC) method is useful because it does not require storing the transfer-matrix or a complete vector in computer memory. We work with transfer-matrices up to a dimension of approximately  $10^{11} \times 10^{11}$  corresponding to a system width of 24 tiles. Although we can use much larger system sizes than with the ordinary, numerically exact transfer matrix technique, the price is the introduction of random statistical errors.

In section 2 we introduce notation and review results of earlier work. In particular, we give the relations between the phason strain and the tile densities, the continuum elastic theory of phason fluctuations, and the transfer-matrix formulation for random Penrose tilings [14]. Section 3 contains new analytic results, extending the earlier work, which are technically necessary in implementing the numerical calculation of the entropy and stiffness constants. In particular, we explain the use of chemical potentials to control the phason strain; show a useful identity of the needed value of the chemical potential with the true entropy per unit area; and derive the dependence of the entropy on the transverse phason strain (the variable we control). Nearly identical results are equally valid for the other two-dimensional tilings with ten-fold symmetry. In section 4 we present results and conclusions. We present a numerically precise determination of the entropy per tile (in the ten-fold symmetric state where it is maximized). Using chemical potentials to deviate from this state, and fitting the variation of the entropy to the known form of the quadratic 'phason' elasticity, we extract estimates for the three independent phason stiffness coefficients  $K_+$ ,  $K_-$  and  $K_z$ . (Our approach to the

data analysis is different from that of Widom *et al* [18] who did not separate  $K_+$  and  $K_-$ .) We also discuss the efficacy of the TMMC method as compared with standard Monte Carlo simulation, or the finite-size scaling of exact transfer-matrix computations for small systems. Appendix A provides the basic theory of the transfer-matrix Monte Carlo method and presents details of the implementation which may be applied to any TMMC calculation. Appendix B presents the particulars of our TMMC implementation for the random Penrose tiling, and discusses our attempts to improve the convergence of the method with importance sampling. Appendix C summarizes useful information about the random tiling of  $60^\circ$  rhombi.

## 2. Basic theory of random Penrose tilings<sup>†</sup>

### 2.1. Physical and phason space

A random Penrose tiling (i.e. a tiling of  $36^\circ$  and  $72^\circ$  rhombi, see figure 1) may be viewed as the projection of a connected two-dimensional hypersurface made of 2-faces of a five-dimensional simple cubic lattice. Each vertex of the tiling is specified by a vector

$$\mathbf{r}^{\parallel} = \sum_{\alpha=1}^5 n_{\alpha} \mathbf{e}_{\alpha}^{\parallel} \quad (1)$$

where  $n_{\alpha}$  are integers and

$$\mathbf{e}_{\alpha}^{\parallel} = (-\sin(2\pi\alpha/5), \cos(2\pi\alpha/5)) \quad (2)$$

as shown in figure 1. Types of tiles are specified by their edge directions. For instance, tiles with edge directions  $\mathbf{e}_1^{\parallel}$  and  $\mathbf{e}_3^{\parallel}$  are called (1, 3) (or (3, 1)) tiles. The  $(\alpha, \alpha+1)$  and  $(\alpha, \alpha+2)$  tiles are termed thin and fat tiles respectively. The (1, 3) and (1, 4) tiles will be called thin vertical tiles, and (3, 4) and (2, 5) tiles will be called fat vertical and thin horizontal tiles respectively.

The  $\mathbf{e}_{\alpha}^{\parallel}$  vectors are projections onto the two-dimensional 'physical space' of the basis vectors of a five-dimensional cubic lattice. The corresponding 'phason' coordinate of the vertex (1) is

$$\mathbf{r}^{\perp} = \sum_{\alpha=1}^5 n_{\alpha} \mathbf{e}_{\alpha}^{\perp} \quad (3)$$

where<sup>‡</sup>

$$\mathbf{e}_{\alpha}^{\perp} = (-\sin(4\pi\alpha/5), \cos(4\pi\alpha/5), 1/\sqrt{2}) \quad (4)$$

and the five-dimensional position is

$$\begin{aligned} \mathbf{r}^{\perp} + \mathbf{r}^{\parallel} &= \sum_{\alpha=1}^5 n_{\alpha} (\mathbf{e}_{\alpha}^{\perp} + \mathbf{e}_{\alpha}^{\parallel}) \\ &= \sum_{\alpha=1}^5 n_{\alpha} \mathbf{e}_{\alpha}. \end{aligned} \quad (5)$$

<sup>†</sup> Corrections to a number of errors in [14] are listed here. The  $(d/D)$  of (2.6) should be replaced with a  $(d/D)^2$ , the 0.9960 in (4.6) should be replaced with 1.2892, the 0.95 in (4.7) should be replaced with 0.8123 and (4.8) should read  $(L/N_L) = 5/2\tau^2 = 0.9549$ . A numerically incorrect entropy value (corrected in our (68)) is quoted at the end of section 3.2.

<sup>‡</sup> The more common definition replaces  $4\pi\alpha/5 \rightarrow 6\pi\alpha/5$  in (4); this merely changes the sign of the  $x^{\perp}$  components of all phason vectors.

2.2. Phason strain and tile densities

The long wavelength behaviour of the hypersurface is described by the coarse grained phason coordinate

$$\mathbf{h}(\mathbf{r}^{\parallel}) = \langle \mathbf{r}^{\perp} \rangle_{\mathbf{r}^{\parallel}} \tag{6}$$

where  $\langle \dots \rangle_{\mathbf{r}^{\parallel}}$  signifies averaging in the vicinity of  $\mathbf{r}^{\parallel}$  over a region large in comparison with the tile size. (Henceforth we abbreviate  $\mathbf{r}^{\parallel}$  as  $\mathbf{r}$ .) The phason strain tensor is given by

$$\mathbf{E}(\mathbf{r}) = \nabla_{\mathbf{r}} \mathbf{h}(\mathbf{r}). \tag{7}$$

For uniform phason strain  $\mathbf{E}(\mathbf{r}) = \mathbf{E}$ ,

$$\mathbf{h} + \mathbf{r} = \mathbf{E}\mathbf{r} + \mathbf{r} = \left\langle \sum_{\alpha=1}^5 n_{\alpha} \mathbf{e}_{\alpha} \right\rangle_{\mathbf{r}} \tag{8}$$

so the hyperplane may be parameterized by  $\langle n_{\alpha} \rangle_{\mathbf{r}} = \mathbf{m}_{\alpha} \cdot \mathbf{r}$  where

$$\mathbf{m}_{\alpha} = \nabla_{\mathbf{r}} \langle n_{\alpha} \rangle_{\mathbf{r}} = \frac{2}{5} (\mathbf{e}_{\alpha}^{\parallel} + \mathbf{e}_{\alpha}^{\perp} \mathbf{E}). \tag{9}$$

Now let us consider a large parallelogram in the physical space with edge vectors  $\mathbf{p}_{\alpha}$  and  $\mathbf{p}_{\beta}$ , and area  $|\mathbf{p}_{\alpha} \times \mathbf{p}_{\beta}|$ , such that  $\mathbf{p}_{\alpha} \cdot \mathbf{m}_{\alpha} = \mathbf{0}$  and  $\mathbf{p}_{\beta} \cdot \mathbf{m}_{\beta} = \mathbf{0}$ . This defines a parallelogram on the hyperplane whose projection onto the  $\mathbf{e}_{\alpha}, \mathbf{e}_{\beta}$  plane is a square of area  $(\mathbf{p}_{\alpha} \cdot \mathbf{m}_{\beta})(\mathbf{p}_{\beta} \cdot \mathbf{m}_{\alpha})$  in units of  $|\mathbf{e}_{\alpha} \times \mathbf{e}_{\beta}| = \frac{5}{2}$ . Therefore  $n_{\alpha\beta}$ , the number of  $(\alpha, \beta)$  tiles per unit area, [14] is

$$n_{\alpha\beta} = \frac{(\mathbf{p}_{\alpha} \cdot \mathbf{m}_{\beta})(\mathbf{p}_{\beta} \cdot \mathbf{m}_{\alpha})}{|\mathbf{p}_{\alpha} \times \mathbf{p}_{\beta}|} = |\mathbf{m}_{\alpha} \times \mathbf{m}_{\beta}|. \tag{10}$$

Note that  $n_{\alpha\beta}$  has terms up to quadratic in  $\mathbf{E}$ . For future reference we present the first-order expansions

$$n_{34} \approx (2\sqrt{3} - \tau/25)[1 - E_{xx}(\tau + 1) + E_{yy}(1 - \tau) - \sqrt{2}E_{zy}] \tag{11}$$

$$n_{52} \approx (2\sqrt{3} - \tau/25)[\tau + E_{xx}(\tau - 1) - E_{yy}(1 + \tau) + \sqrt{2}E_{zy}]. \tag{12}$$

The complete and exact expression for the total tile density is

$$n_{\text{tile}} = \sum_{\alpha\beta} n_{\alpha\beta} = n_{\text{tile}}^0 [1 - (E_{xx}E_{yy} - E_{yx}E_{xy})/\tau^3] \tag{13}$$

where the first/second subscript of  $E$  is the phason/physical space index, and

$$n_{\text{tile}}^0 = n_{\text{tile}}(\mathbf{E} = \mathbf{0}) = 2\tau^2\sqrt{3} - \tau/5 \approx 1.231. \tag{14}$$

Hereafter, the superscript '0' denotes the  $\mathbf{E} = \mathbf{0}$  value of a variable. Notice that there is no linear  $\mathbf{E}$  term in  $n_{\text{tile}}$ .

2.3. Elasticity theory

The tilings allowed by our packing rules form an ensemble, in which we have given each tiling configuration equal weight. (When we include chemical potentials, as introduced below for technical purposes, different configurations have different weights.) The entropy is proportional to the system size. Thus our fundamental thermodynamic function is the entropy density as a function of phason strain  $S(\mathbf{E})$ . (We will measure this in units of entropy per tile.)

The fundamental conjecture of the random tiling model of quasiperiodic order is that the entropy of the tiling is a quadratic maximum at  $E = 0$ , i.e.

$$S = S^0 - \frac{1}{2}EKE \tag{15}$$

where  $K$ , the stiffness constant tensor, is positive definite [10, 14]. Group theoretic arguments [23] have been used to identify the number of independent components of  $K$ . The functional form of the entropy must be invariant under any rotation of the tiling by a multiple of  $72^\circ$  together with the corresponding rotation about  $z^\perp$  in phason space (which is twice the angle, see (4)). This analysis yields three independent stiffness constants which couple components of the phason strain to give:

$$\begin{aligned} S &= S^0 - \frac{1}{2}K_+[(E_{xx} + E_{yy})^2 + (E_{xy} - E_{yx})^2] \\ &\quad - \frac{1}{2}K_-[(E_{xx} - E_{yy})^2 + (E_{xy} + E_{yx})^2] - K_z[E_{zx}^2 + E_{zy}^2] \\ &= S^0 - (K_+ + K_-)[E_{xx}^2 + E_{yy}^2 + E_{xy}^2 + E_{yx}^2] \\ &\quad - 2(K_+ - K_-)[E_{xx}E_{yy} - E_{xy}E_{yx}] - K_z[E_{zx}^2 + E_{zy}^2]. \end{aligned} \tag{16}$$

This work provides the first estimates of both  $(K_+ + K_-)$  and  $(K_+ - K_-)$  for decagonal quasiperiodic tilings. The  $(K_+ - K_-)$  contribution to the entropy of a region reduces to an integral over the boundary since

$$E_{xx}E_{yy} - E_{xy}E_{yx} = \nabla \times [h_x \nabla h_y] \tag{17}$$

is an exact differential [24]. If one is only interested in the fluctuations about the average phason strain, or if the average phason strain is zero, the  $(K_+ - K_-)$  term may be neglected. (This is equivalent to converting to Fourier components, i.e.  $E_{xx} \rightarrow q_x h_x$ ,  $E_{xy} \rightarrow q_y h_x$ , etc.) Thus, Monte Carlo simulations which determine the (entropic) elastic constants by measuring fluctuations around a state can only measure the combination  $(K_+ + K_-)$ †. This is true whether there is a fixed net phason strain due to the boundary conditions, or whether the system is allowed to find the maximum-entropy state with zero phason strain. Our estimate of the value of  $(K_+ - K_-)$  is of physical importance since, if the global phason strain is not constrained at zero, the sign of  $(K_+ - K_-)$  determines the stability of the zero phason strain random tiling as compared to states with non-zero uniform strain, e.g. large rational approximant crystals with random tiling disorder [16].

#### 2.4. Tiling rules and the transfer-matrix

The nearly horizontal dotted lines across figure 1 separate ‘layers’ of the tiling. The tiling has periodic boundary conditions horizontally. Dotted line segments of length 1,  $1$ ,  $\tau^{-1}$  and  $\tau^{-1}$  along  $e_3^\parallel$ ,  $-e_2^\parallel$ ,  $e_3^\parallel$ , and  $-e_2^\parallel$  are termed  $L^+$ ,  $L^-$ ,  $S^+$  and  $S^-$  steps respectively. For instance, the sequence of steps across the leading (top) layer of figure 1 is  $\{L^+L^+L^-L^-S^+L^-S^-L^+S^+\}$ . Layer lines cut through all thin and fat vertical tiles. A simple counting argument shows that the number of steps per unit area,  $n_{\text{step}} = n(L^+) + n(L^-) + n(S^+) + n(S^-)$ , obeys [14]

$$n_{\text{step}} = n_{\text{tile}} + n_{34} - n_{52}. \tag{18}$$

† But a Monte Carlo simulation with free boundary conditions, could in principle determine  $(K_+ - K_-)$ , if one measures the global phason strain: this fluctuates according to a statistical weight which is exponential in the system area times the full phason elastic term.

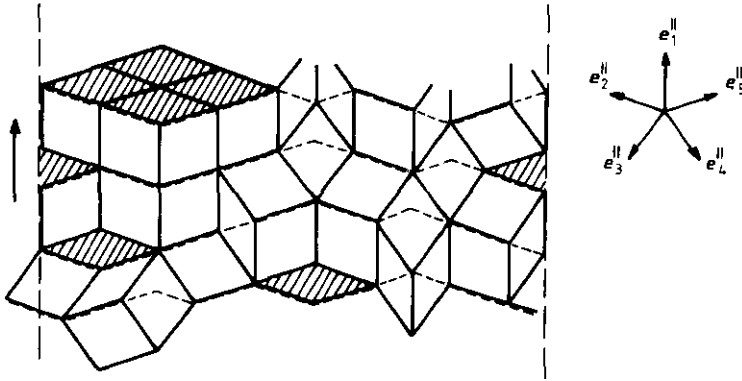


Figure 1. A random Penrose tiling configuration. Layer lines are shown broken. (After figure 4 of [14].)

The transition rules assign a weight to each permissible permutation of steps between two layers. These weights form the entries of the transfer-matrix. The tiling of a new layer is determined by the state of the previous layer and the operations performed in the permutation of steps between layers<sup>†</sup>. The transition rules for generating successive layers may be divided into three stages as follows (see appendix B for TMMC implementation details):

(i) The  $LL$  rule is composed of any number of  $L^+L^- \rightarrow L^-L^+$  exchanges between nearest-neighbour steps. Thus, the  $LL$  rule changes the plus/minus ordering within strings of consecutive  $L$  steps;  $L^+$  steps can move to the right and the  $L^-$  steps can move to the left, but they cannot move past an  $S$ . Each exchange corresponds to adding a thin horizontal tile to the leading edge of the tiling since the bottom surface of the tile is an  $L^-L^+$  pair and the top surface is an  $L^+L^-$  pair. Since thin horizontal tiles are to be assigned a chemical potential  $\mu_{S2}$  to preserve five-fold symmetry (see below), a permutation requiring  $n$  of these exchange operations is given a weight  $e^{n\mu_{S2}}$ .

(ii) The  $SL$  rule is composed of any number of  $S^+L \rightarrow LS^+$  or  $LS^- \rightarrow S^-L$  exchanges between nearest-neighbour steps, where  $L$  refers to either an  $L^+$  or  $L^-$  step, and similarly  $S$  refers to either  $S^+$  or  $S^-$ . The  $SL$  rule can change the ordering of the  $S$  and  $L$  steps across the layer, but clearly cannot change the plus/minus ordering of the  $L$  steps or the  $S$  steps. Each possible permutation of steps is given a weight of unity. The  $SL$  rule determines the positions of thin vertical (1, 4) and (1, 3) tiles in the next layer of the tiling. An added (1, 4) tile, for instance, is positioned so that its lower vertex is  $n$  vertices to the right of the right-hand edge of the corresponding  $S^+$  in the layer below, where  $n$  is the number of  $S^+L \rightarrow LS^+$  exchanges applied. Gaps between thin vertical tiles are filled in by a single layer of (1, 2), (1, 5), (3, 5) and (2, 4) tiles in a manner which maintains the ordering of  $L$  steps from the layer below.

(iii) The  $SS$  rule is composed of  $S^+S^- \rightarrow S^-S^+$  nearest-neighbour exchanges, but unlike the previous rules each  $S$  step can undergo at most one  $SS$  exchange per layer. The  $SS$  exchange corresponds to the substitution of a fat vertical tile for a (1, 4), (1, 3) pair of thin vertical tiles; the lower contour of a fat vertical tile is the same as that of a (1, 4), (1, 3) pair, and the upper contour is the same as that of a (1, 3), (1, 4) pair. Since fat vertical tiles are to be assigned a chemical potential  $\mu_{34}$  to preserve five-fold

<sup>†</sup> The mapping of step permutations to tilings is not unique when there are no thin vertical tiles, but this is far from the condition of five-fold symmetry and will not concern us here.

symmetry (see below), the weight of a permutation is  $e^{n\mu_{34}}$  where  $n$  is the number of  $SS$  exchanges.

The transfer-matrix  $T$  is equal to the product

$$T = T_{SS}T_{SL}T_{LL} \quad (19)$$

where the entries of  $T_{SL}$ ,  $T_{LL}$ , and  $T_{SS}$  are determined by the  $SL$ ,  $LL$ , and  $SS$  rules. Because the entropy is related to  $\text{Tr } T^N$  (see below), cyclic permutations of the matrices in the product of equation (19) do not affect the entropy. The matrices  $T_{SS}$  and  $T_{LL}$  commute, since the application of the  $SS$  rule has no effect on the application of the  $LL$  rule, and vice versa. Therefore we are free to permute the order of multiplication of the matrices in (19). Reordering of the matrices does affect how the layer lines are drawn in figure 1; the layer lines go above/below groups of horizontal thin tiles when  $T_{LL}$  comes after/before  $T_{SL}$  in the product defining  $T$ .

The number of steps of each type across a layer will be termed the 'transverse boundary condition'. Since the transition rules only involve permutations of steps, the number of  $L^+$ ,  $L^-$ ,  $S^+$  and  $S^-$  steps per layer ( $N(L^+)$ ,  $N(L^-)$ ,  $N(S^+)$  and  $N(S^-)$ ) is conserved and the transverse boundary conditions (to be denoted as  $\{N(L^+), N(L^-), N(S^+), N(S^-)\}$ ) across each layer are the same. The net displacement upon traversing the steps of a layer (transversely),

$$\begin{aligned} w_x^{\parallel} &= \sin(2\pi/5) \left[ (N(L^+) + N(L^-)) + \frac{1}{\tau} (N(S^+) + N(S^-)) \right] \\ w_y^{\parallel} &= \cos(2\pi/5) \left[ (N(L^+) - N(L^-)) + \frac{1}{\tau} (N(S^+) - N(S^-)) \right] \end{aligned} \quad (20)$$

and the corresponding phason space displacement

$$\begin{aligned} w_x^{\perp} &= \sin(2\pi/5) \left[ (-N(S^+) - N(S^-)) + \frac{1}{\tau} (N(L^+) + N(L^-)) \right] \\ w_y^{\perp} &= (1 + \cos(2\pi/5)) \left[ (N(S^+) - N(S^-)) + \frac{1}{\tau} (-N(L^+) + N(L^-)) \right] \\ w_z^{\perp} &= \frac{1}{\sqrt{2}} [2N(S^+) - 2N(S^-) + N(L^+) - N(L^-)] \end{aligned} \quad (21)$$

is therefore determined by the transverse boundary conditions. For ease of reference, table 1 lists  $w^{\parallel}$  and  $w^{\perp}$  for a number of transverse boundary conditions. Notice that

Table 1. Displacements across strips.

Initial conditions	$w_x^{\parallel}$	$w_y^{\parallel}$	$w_x^{\perp}$	$w_y^{\perp}$	$w_z^{\perp}$
$\{n, n, n, n\}$	3.08	0	-0.727	0	0
$\{2n, 2n, n, n\}$	4.98	0	0.449	0	0
$\{3n, 3n, 2n, 2n\}$	8.06	0	-0.278	0	0
$\{3n, 3n, n, n\}$	6.88	0	1.63	0	0
$\{5n, 5n, 3n, 3n\}$	13.04	0	0.17	0	0
$\{5n, 5n, 2n, 2n\}$	11.86	0	2.07	0	0
$\{4n, 4n, 3n, 3n\}$	11.14	0	-1.00	0	0
$\{3n, 4n, 2n, 2n\}$	9.01	-0.309	0.310	0.809	-0.707



when  $N(L+) = N(L-)$  and  $N(S+) = N(S-)$ , only  $w_x^{\parallel}$  and  $w_x^{\perp}$  are non-zero. In general, the choice of transverse boundary conditions imposes three restrictions on  $E$  for any given system corresponding to the three components of the equation

$$w^{\perp} = Ew^{\parallel}. \tag{22}$$

### 3. Implementation and related theory

#### 3.1. The functional form of the entropy

The TMMC method allows the determination of the largest eigenvalue  $\lambda_0$  of the transfer-matrix. The entropy per layer  $S_{\text{lay}}$  is related to  $\lambda_0$  by

$$S_{\text{lay}} = \ln \lambda_0. \tag{23}$$

There is no physical significance to our definition of layers; the quantity of interest is actually the entropy per unit area  $S$ , where

$$S_{\text{lay}}/N_w = S/n_{\text{step}} \tag{24}$$

and

$$N_w = N(L+) + N(L-) + N(S+) + N(S-) \tag{25}$$

is the number of steps across the width of the system, a constant. The largest eigenvalue  $\lambda_0$  is in effect a maximization of the entropy with respect to  $E_{xy}$ ,  $E_{yy}$ , and  $E_{zy}$  with the ‘transverse boundary condition’ held fixed.

Because  $n_{\text{step}}$  is a function of  $E$ ,  $S_{\text{lay}}$  is not simply proportional to  $S$  and the maxima of  $S_{\text{lay}}$  and  $S$  occur at different values of the phason strain. To manipulate the phason strain so as to allow exploration of the functional dependence of  $S_{\text{lay}}$  near the phason strain corresponding to the maximum of  $S$ , we modify equations (15) and (16) by introducing the chemical potentials  $\mu_{34}$  and  $\mu_{52}$ , i.e. we generalize the entropy to the free energy

$$F = S^0 - \frac{1}{2} EKE - \mu_{34}n_{34} - \mu_{52}n_{52}. \tag{26}$$

When

$$\mu_{52} = -\mu_{34} = \mu^0 \equiv S^0/n_{\text{tile}}^0 \tag{27}$$

the second-order expansion of (24), using equations (26) and (18) is

$$F_{\text{lay}}/N_w = \mu^0 - \frac{1}{2n_{\text{step}}^0} EK'E \tag{28}$$

where  $n_{\text{step}}^0 \approx 1.29$  is the value of (18) at  $E = \mathbf{0}$ ; here  $EK'E$  has the same functional form as equation (16) with

$$K'_{\pm} = K_{\pm} \mp \beta\mu^0 \tag{29}$$

$$K'_z = K_z \tag{30}$$

where for convenience we have defined  $\beta \equiv n_{\text{tile}}^0/\tau^3 = 0.29$ .

In other words, if  $\mu_{52}$  and  $\mu_{34}$  have the special values given by (27), then (28) says that  $F_{\text{lay}}$  has a maximum at the same phason strain ( $E = \mathbf{0}$ ) as  $S$  does, and furthermore that at that phason strain  $F_{\text{lay}}/N_w$  equals the entropy per tile  $\mu_0$ . Thus, small variations

of  $w^\perp/w^\parallel$  about zero, and  $\mu_{52}$  and  $-\mu_{34}$  about  $\mu^0$  therefore allow the determination of the functional form of  $F_{lay}/N_w$  (and consequently that of  $S$ ) about  $E=0$ . Using equations (11)-(13), (18), and (24)-(30), the expansion of  $F_{lay}/N_w$  to second order for general  $\mu_{34}$  and  $\mu_{52}$  is

$$F_{lay}/N_w = \mu^0 - \frac{1}{n_{step}^0} [\frac{1}{2}EK'E + \psi_{xx}E_{xx} + \psi_{yy}E_{yy} + \psi_{zy}E_{zy}] \tag{31}$$

where  $\delta\mu_{52} = \mu^0 - \mu_{52}$ , where

$$\begin{aligned} \psi_{xx} &= \frac{2\sqrt{3-\tau}}{25} \left[ -\delta\mu_{34} \left( \frac{4\tau+3}{\tau^3} \right) + \delta\mu_{52} \left( \frac{3\tau+1}{\tau^4} \right) \right] \approx -0.2103\delta\mu_{34} + 0.0803\delta\mu_{52} \\ \psi_{yy} &= \frac{2\sqrt{3-\tau}}{25} \left[ -\delta\mu_{34} \left( \frac{\tau+2}{\tau^3} \right) - \delta\mu_{52} \left( \frac{8\tau+6}{\tau^4} \right) \right] \approx -0.0803\delta\mu_{34} - 0.2599\delta\mu_{52} \\ \psi_{zy} &= \frac{\sqrt{2}\sqrt{3-\tau}}{25} \left[ -\delta\mu_{34} \left( \frac{3\tau+1}{\tau^3} \right) + \delta\mu_{52} \left( \frac{11\tau+7}{\tau^4} \right) \right] \approx -0.0919\delta\mu_{34} + 0.2406\delta\mu_{52} \end{aligned} \tag{32}$$

with  $\delta\mu_{34} = -\mu^0 - \mu_{34}$ .

The value of  $F_{lay}/N_w$  is proportional to the maximum eigenvalue of  $T$ . Therefore, the expected form of  $F_{lay}/N_w$  as a function of  $\mu_{52}$ ,  $\mu_{34}$ ,  $w^\perp$ , and  $w^\parallel$  is found by maximizing equation (31) with respect to  $E$  subject to the transverse-boundary-condition constraints (22). This calculation is facilitated by the definitions:

$$v^\parallel = \frac{1}{\sqrt{2}} \begin{pmatrix} w_x^\parallel & w_y^\parallel & w_x^\parallel & w_y^\parallel & 0 & 0 \\ w_y^\parallel & -w_x^\parallel & -w_y^\parallel & w_x^\parallel & 0 & 0 \\ 0 & 0 & 0 & 0 & \sqrt{2}w_x^\parallel & \sqrt{2}w_y^\parallel \end{pmatrix} \tag{33}$$

$$\Psi^T = \left( \frac{\psi_{xx} + \psi_{yy}}{\sqrt{2}}, 0, \frac{\psi_{xx} - \psi_{yy}}{\sqrt{2}}, 0, 0, \psi_z \right) \tag{34}$$

$$k = \text{diag}(K'_+, K'_+, K'_-, K'_-, K_z, K_z) \tag{35}$$

and

$$\begin{aligned} g_1 &= \frac{E_{xx} + E_{yy}}{\sqrt{2}} & g_2 &= \frac{E_{xy} - E_{yx}}{\sqrt{2}} \\ g_3 &= \frac{E_{xx} - E_{yy}}{\sqrt{2}} & g_4 &= \frac{E_{yx} + E_{xy}}{\sqrt{2}} \\ g_5 &= E_{zx} & g_6 &= E_{zy}. \end{aligned} \tag{36}$$

With these definitions equation (31) may be re-expressed in matrix form as

$$[(F_{lay}/N_w) - \mu^0]n_{step}^0 - \delta\mu_{34}n_{34}^0 - \delta\mu_{52}n_{52}^0 = \frac{1}{2}g^Tkg + \Psi^Tg \tag{37}$$

and the constraint (22) becomes

$$w^\perp = v^\parallel g. \tag{38}$$

The right-hand side of equation (37) contains all the  $E$  dependence. After considerable calculation we determine that the solution of minimizing equation (37) subject to

constraint (38) is

$$\begin{aligned}
 (F_{1ay}/N_W) = & \mu^0 + (\delta\mu_{34}n_{34}^0 + \delta\mu_{52}n_{52}^0)/n_{\text{step}}^0 + \frac{1}{n_{\text{step}}^0(w_x^{\parallel 2} + w_y^{\parallel 2})} \\
 & \times \left[ \frac{\psi_{xx}^2 w_y^{\parallel 2} + \psi_{yy}^2 w_x^{\parallel 2}}{K_+ + K_-} + \frac{\psi_{zy}^2 w_x^{\parallel 2}}{2K_z} - \frac{1}{2} K_z w_z^{\perp 2} \right. \\
 & + w_x^{\parallel} w_x^{\perp} \left( \psi_{xx} + \psi_{yy} \frac{K_- - K_+ + 2\beta\mu^0}{K_+ + K_-} \right) \\
 & + w_y^{\parallel} w_y^{\perp} \left( \psi_{yy} + \psi_{xx} \frac{K_- - K_+ + 2\beta\mu^0}{K_+ + K_-} \right) \\
 & \left. - (w_x^{\perp 2} + w_y^{\perp 2}) \frac{(K_+ - \beta\mu^0)(K_- + \beta\mu^0)}{K_+ + K_-} \right]. \tag{39}
 \end{aligned}$$

The requirement of an entropy maximum at  $\delta\mu_{34} = \delta\mu_{52} = 0$  restricts  $((K_+ - \beta\mu^0) \times (K_- + \beta\mu^0))/(K_+ + K_-)$  and  $K_z$  to positive values. Since much of the analysis of numerical results will consider systems where  $w_y^{\perp} = w_z^{\perp} = w_y^{\parallel} = 0$ , for ease of reference we display the form of equation (39) under these conditions:

$$\begin{aligned}
 (F_{1ay}/N_W) = & \mu^0 + (\delta\mu_{34}n_{34}^0 + \delta\mu_{52}n_{52}^0)/n_{\text{step}}^0 \\
 & + \frac{1}{n_{\text{step}}^0} \left[ \psi_{yy}^2/(K_+ + K_-) + \psi_{zy}^2/(2K_z) \right. \\
 & + (w_x^{\perp}/w_x^{\parallel}) \left( \psi_{xx} + \psi_{yy} \frac{K_- - K_+ + 2\beta\mu^0}{K_+ + K_-} \right) \\
 & \left. - (w_x^{\perp 2}/w_x^{\parallel 2}) \frac{(K_+ - \beta\mu^0)(K_- + \beta\mu^0)}{K_+ + K_-} \right]. \tag{40}
 \end{aligned}$$

#### 4. Results and conclusions

The transfer-matrix Monte Carlo method is described in appendix A; the implementation of the transfer-matrix for the random Penrose tiling [14] is outlined in appendix B. Due to practical limitations, we are restricted to calculating  $F_{1ay}/N_W$  for systems with  $N_W \leq 24$  (see appendix A) so it is necessary to apply finite-size scaling to the TMMC data. Each TMMC run produces an estimate of  $F_{1ay}/N_W$  for a given  $w^{\perp}$ ,  $w^{\parallel}$ ,  $\mu_{34}$  and  $\mu_{52}$ . Each infinite size extrapolation (see table 2) for a given  $w^{\perp}/w^{\parallel}$  is based on finite-size scaling of the results for two system sizes.

To fit for the maximum entropy density  $S^0$  and the stiffness constants  $K_+$ ,  $K_-$  and  $K_z$ , we will use the expansions (39) and (40) from section 3. These expansions depend on  $\mu_0$ ; however, this is proportional to the entropy  $S_0$  and so it is one of the objects of the calculation. In principle we can find  $\mu_0$  self-consistently because  $F_{1ay}/N_W$  must equal  $\mu_0$ , but we need a preliminary estimate for  $\mu^0$  (section 4.1), so that we can limit our fits to data in the vicinity of  $E = 0$  where equation (39) is valid. (Since the transverse boundary condition forces a finite phason strain, the validity of the quadratic expansion (39) is problematical, see section 4.2).

**Table 2.** Infinite-size extrapolations of the TMMC data.

Entry	Initial conditions	$-\mu_{34}$	$\mu_{52}$	$S_{lay}/N_W$
a	{3n, 3n, 2n, 2n}	0.4805	0.4805	0.4810 (7)
b	{3n, 3n, 2n, 2n}	0.4750	0.4750	0.4805 (6)
c	{3n, 3n, 2n, 2n}	0.5812	0.5812	0.4874 (2)
d	{3n, 3n, 2n, 2n}	0.3812	0.3812	0.4758 (5)
e	{3n, 3n, 2n, 2n}	0.5812	0.3812	0.5006 (3)
f	{3n, 3n, 2n, 2n}	0.3812	0.5812	0.4624 (2)
g	{3n, 3n, 2n, 2n}	0.4805	0.3305	0.4919 (2)
h	{3n, 3n, 2n, 2n}	0.4805	0.6305	0.4717 (4)
i	{3n, 3n, 2n, 2n}	0.3305	0.4805	0.4627 (3)
j	{3n, 3n, 2n, 2n}	0.6305	0.4805	0.4999 (4)
k	{3n, 3n, 2n, 2n}	0.6305	0.6305	0.4906 (3)
l	{2n, 2n, n, n}	0.4805	0.4805	0.4800 (7)
m	{2n, 2n, n, n}	0.5805	0.5805	0.4813 (4)
n	{2n, 2n, n, n}	0.3805	0.3805	0.4793 (4)
o	{2n, 2n, n, n}	0.5805	0.3805	0.5001 (2)
p	{2n, 2n, n, n}	0.3805	0.5805	0.4609 (3)
q	{2n, 2n, n, n}	0.3305	0.4805	0.4648 (2)
r	{3n, 4n, 2n, 2n}	0.4810	0.4810	0.4793 (3)
s	{n, n, n, n}	0.4805	0.4805	0.4745 (2)
t	{3n, 3n, n, n}	0.4805	0.4805	0.4698 (2)

**4.1. Finite-size scaling and preliminary estimates**

The finite-size scaling behaviour of  $F_{lay}/N_W$  with  $N_W$  satisfies

$$\left[ F_{lay}/N_W - \lim_{N_W \rightarrow \infty} (F_{lay}/N_W) \right] \approx c/N_W^2 \tag{41}$$

where  $c$  is a function of  $w^\perp/w^\parallel$ ,  $\mu_{34}$  and  $\mu_{52}$ . This scaling form is consistent with capillary wave theory [25], the six-fold symmetric random tiling of the 60° rhombi (see appendix C and [26]) and the data of Widom *et al* [18]. To illustrate the smallness of the corrections to the finite-size scaling form, figure 2 displays  $F_{lay}/N_W$  against  $N_W^{-2}$

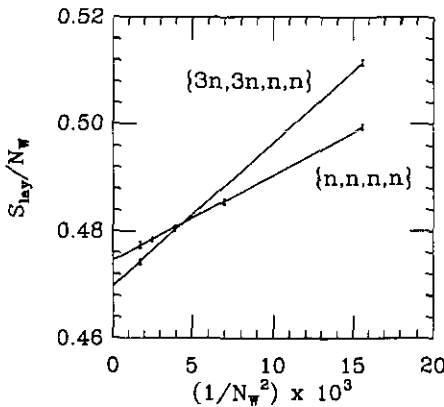


**Figure 2.** Finite size behaviour of  $F_{lay}/N_W$  for  $\{n, n, n, n\}$  and  $\{3n, 3n, n, n\}$  systems for  $\mu_{52} = -\mu_{34} = 0.4805$ . The error bars of the  $\{3n, 3n, n, n\}$  data points and the two right-hand  $\{n, n, n, n\}$  data points are magnified for clarity.

for two systems:  $\{n, n, n, n\}$  layers with  $n=2, \dots, 6$ , and  $\{3n, 3n, n, n\}$  layers with  $n=1, 2, 3$ , where  $\mu_{52} = -\mu_{34} = 0.4805$ . Table 2 displays least-squares infinite size extrapolations of the TMMC data using equation (41). The  $n \rightarrow \infty$  extrapolations for  $\{3n, 3n, 2n, 2n\}$  systems utilized  $F_{\text{lay}}/N_W$  data from  $\{3, 3, 2, 2\}$  and  $\{6, 6, 4, 4\}$  systems, and the  $\{2n, 2n, n, n\}$  extrapolations utilized  $\{4, 4, 2, 2\}$  and  $\{8, 8, 4, 4\}$  systems.

To explore the quadratic maximum of  $S$  and determine  $S^0, K_+, K_-$  and  $K_z$  we must locate the value of  $\mu^0$ . For simplicity let us consider  $\{n, n, m, m\}$  layers so that  $w_x^\perp = w_y^\perp = w_x^\parallel = 0$ . In view of equation (27), it is natural to restrict ourselves to the line  $\mu_{52} = -\mu_{34} = \mu$ ; when we speak of  $F_{\text{lay}}/N_W$  as a function of  $\mu$ , this is to be understood. For notational convenience we now define a modified

$$\frac{\bar{F}_{\text{lay}}}{N_W} \equiv \left[ \frac{F_{\text{lay}}}{N_W} + \frac{1}{n_{\text{step}}^0} \left( \frac{w_x^\perp}{w_x^\parallel} \right)^2 \frac{(K_+ - \beta\mu^0)(K_- + \beta\mu^0)}{n_{\text{step}}^0(K_+ + K_-)} \right]. \tag{42}$$

Examination of equation (40) shows that

$$\left. \frac{\bar{F}_{\text{lay}}(\mu)}{N_W} \right|_{\mu=\mu^0} = \mu. \tag{43}$$

That is, if we plot the graph of the function  $\bar{F}_{\text{lay}}(\mu)/N_W$  against  $\mu$ , this curve will intersect the line through the origin with unit slope at  $(\mu_0, \mu_0)$ . Since the definition (42) of  $\bar{S}/N_W$  depends upon  $\mu_0$ , this might not seem helpful; however, it turns out that the intersection of this line with the unmodified curve  $F_{\text{lay}}(\mu)$ , as illustrated in figure 3, gives a very good estimate of  $\mu_0$ . For

$$\frac{(K_+ - \beta\mu^0)(K_- + \beta\mu^0)}{(K_+ + K_-)} \leq 0.2$$

(see below), and for the  $\{3n, 3n, 2n, 2n\}$  data,  $(1/n_{\text{step}}^0)(w_x^\perp/w_x^\parallel)^2 \approx 0.001$ . Consequently, the shift  $(\bar{F}_{\text{lay}} - F_{\text{lay}})/N_W$  due to the extra term in (42) is near the resolution of figure 3, even with its expanded vertical scale, and the  $\mu$  values of the intersections of the line with  $F_{\text{lay}}/N_W$  and with  $\bar{F}_{\text{lay}}/N_W$  are indistinguishable. Thus we extract the preliminary estimate

$$\mu^0 = 0.4812 \pm 0.0007 \tag{44}$$

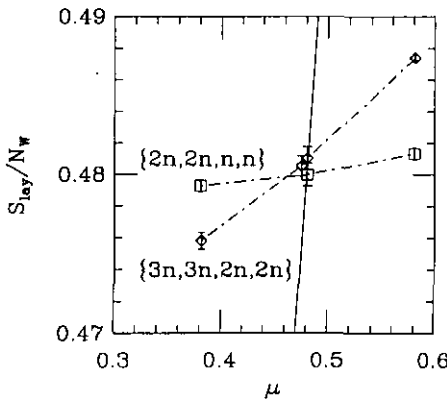


Figure 3. Entropy as a function of  $\mu_{52} = -\mu_{34} = \mu$ . The  $\mu$  value at which the  $\{3n, 3n, 2n, 2n\}$  data crosses the line of unit slope through the origin (full line) provides an estimate of  $\mu^0$ .

from the intersection of the  $\{3n, 3n, 2n, 2n\}$  data (chain) in figure 3 with the line of slope one through the origin (full).

A comparison of the  $\mu = 0.4805$  values of  $F_{lay}/N_w$  for the  $\{3n, 3n, 2n, 2n\}$  and  $\{2n, 2n, n, n\}$  data points (see figure 3 or entries (a) and (l) of table 2) provides a bound on  $((K_+ - \beta\mu^0)(K_- + \beta\mu^0))/(K_+ + K_-)$ . Because we believe that  $\mu = 0.4805$  is within 0.001 of  $\mu^0$ , we expect from (32) that the  $\psi$ 's are of order 0.0002. Assuming that the coefficients of the  $(w_x^+ / w_x^0)^2$ ,  $(w_x^+ / w_x^0)\psi$ , and  $\psi^2$  terms in equation (40) are of order unity or less (see below), the main contribution to the difference between the two data points must come from the term quadratic in  $(w_x^+ / w_x^0)$ . Noting that  $1/n_{step}^0(w_x^+ / w_x^0)^2 \approx 0.008$  and 0.001 for the  $\{2n, 2n, n, n\}$  and  $\{3n, 3n, 2n, 2n\}$  systems respectively, the difference of less than 0.002 between the two points implies the bound

$$\frac{(K_+ - \beta\mu^0)(K_- + \beta\mu^0)}{(K_+ + K_-)} < 0.2. \quad (45)$$

#### 4.2. The higher-order terms problem

Unfortunately, the range over which  $F_{lay}/N_w$  is adequately described by equation (39) is severely limited. This is exemplified by the difference of  $4.7 \times 10^{-3}$  in the values of  $F_{lay}/N_w$  for the  $\{n, n, n, n\}$  and  $\{3n, 3n, n, n\}$  systems at  $\mu_{52} = -\mu_{34} = 0.4805$  (entries (s) and (t) in table 2). As elaborated in appendix C, this difference cannot be attributed to any of the terms in equation (40) since the magnitude of  $w_x^+ / w_x^0$  for both transverse boundary conditions is the same although the sign differs, and since the values of  $\mu_{34}$  and  $\mu_{52}$  are also the same, the only candidate is the term linear in  $w_x^+ / w_x^0$ . However, this term is about two orders of magnitude too small since  $|w_x^+ / w_x^0| \approx 0.236$ , and with the assumption that  $|(K_- - K_+ + 2\beta\mu^0)/K_+ + K_-|$  is of order unity (see below), then the terms linear in  $w_x^+ / w_x^0$  have a magnitude of about  $7 \times 10^{-5}$ . If we ascribe the discrepancy to terms of cubic order or higher in  $w^+ / w^0$ , then the magnitude of these terms becomes of the order of the random error ( $\approx 4 \times 10^{-4}$ ) when  $|w^+ / w^0| \approx 0.1$ .

The restrictions  $|w^+ / w^0| < 0.1$  and  $N_w \leq 24$  severely limit the viable transverse boundary conditions since we need at least two system sizes with the same phason strain to apply finite-size scaling (see table 1)†. For instance, we cannot use  $\{5n, 5n, 3n, 3n\}$  systems because the  $\{10, 10, 6, 6\}$  system is prohibitively large.

#### 4.3. Fitting results

The values of  $K_+$ ,  $K_-$ ,  $K_z$  and  $\mu^0$  have been estimated by nonlinear least squares fits of subsets of the top seventeen entries in table 2 to equation (39). The results of these fits are displayed in table 3. The fitting parameters in the top part of the table are  $(K_+ + K_-)$ ,  $(K_+ - K_-)$ ,  $K_z$  and  $\mu^0$ . The large covariance between the  $(K_+ + K_-)$  and  $(K_+ - K_-)$  estimates prompts the display of the fitting results in terms of  $K_+$ ,  $K_-$ ,  $K_z$  and  $\mu^0$  at the bottom of table 3. The goodness of fit is displayed in the right-hand column. Starred parameters are constrained at either the central value of the estimates by Strandburg *et al* [19] ( $(K_+ + K_-) = 0.60 \pm 0.02$  and  $K_z = 0.56 \pm 0.03$ ), or at the high or low end of the error bars so as to test the sensitivity of the fits to the constrained parameters. The data points (k), (q) and (r) apparently lie outside the region described

† If we were to calculate  $F_{lay}/N_w$  for one system size at each phason strain value, and utilize the phason strain and stiffness constant dependence of the finite-size scaling form, the infinite size extrapolations and the fit to equation (39) would have to be done simultaneously. This has not been attempted here.

**Table 3.** Least-squares fits for  $\mu^0$  and the stiffness constants. Starred parameters are constrained.

Points	$\mu^0$	$K_+ + K_-$	$K_+ - K_-$	$K_z$	Goodness
a-j, l-p, k	0.4732 (2)	0.165 (5)	0.40 (1)	0.140 (5)	0.00
a-j, l-p, q	0.4813 (2)	1.6 (2)	1.4 (2)	1.5 (8)	0.000 05
a-j, l-p, r	0.4809 (2)	1.8 (4)	1.6 (3)	0.51 (9)	0.000 05
a-j, l-p	0.4812 (2)	1.8 (3)	1.5 (3)	0.9 (3)	0.06
a, b, g-j, l-p	0.4713 (3)	1.6 (3)	1.3 (3)	3 ± 6	0.24
a-f, l-p	0.4809 (3)	1.4 (3)	1.2 (3)	0.53 (15)	0.07
a, g-j, l-p	0.4806 (1)	1.2*	1.08 (5)	0.56*	0.008
a-f, l-p	0.4808 (1)	1.2*	0.99 (6)	0.56*	0.1
a-f, l-p	0.4808 (1)	1.2*	0.99 (6)	0.59*	0.1
a-f, l-p	0.4808 (1)	1.24*	1.03 (6)	0.56*	0.1
a-f, l-p	0.4807 (2)	1.2*	1.00 (6)	0.5 (1)	0.07
a-f, l-p	0.4809 (2)	1.5 (3)	1.2 (2)	0.56*	0.1

Points	$\mu^0$	$K_+$	$K_-$	$K_z$	Goodness
a-j, l-p	0.4812 (2)	1.7 (3)	0.14 (4)	0.9 (3)	0.06
a, b, g-j, l-p	0.4713 (3)	1.5 (1)	0.13 (4)	3 ± 6	0.24
a-f, l-p	0.4809 (3)	1.3 (3)	0.12 (4)	0.53 (15)	0.07

by equation (39) since the goodness of fit of the first three entries in table 3 is extremely low; the entropy and stiffness constant estimates must be obtained from data points with smaller magnitudes of  $\psi$  and  $w^\perp/w^\parallel$ .

The  $\mu^0$  estimates from the remaining constrained and unconstrained fits are very accurate and consistent, though the graphical estimate of  $\mu^0$  may be more trustworthy since the least-squares fits may be biased by the higher-order terms in the  $F_{\text{lay}}/N_w$  expansion. We estimate†

$$S^0/n_{\text{tile}}^0 = 0.4810 \pm 0.0005. \quad (46)$$

The estimates for  $K_-$  from constrained and unconstrained fits are very consistent and relatively insensitive to the value of  $K_+$ . Unconstrained fits would indicate  $K_- = 0.13 \pm 0.05$ ; the fits constrained to [19] give the estimate

$$K_- = 0.09 \pm 0.03 \quad (47)$$

which we believe is somewhat more trustworthy. The fitted values of  $K_+$  and  $K_z$  are rather poorly determined; we hypothesize the bounds

$$1 < K_+ < 2 \quad \text{and} \quad 0.4 < K_z < 1.0. \quad (48)$$

The assumptions made earlier in this section concerning the magnitudes of various terms involving the stiffness coefficients are clearly justified. These stiffness constant estimates are consistent with Strandburg *et al* [19].

#### 4.4. Discussion

The marked discrepancy between the accuracy of our stiffness constant estimates and those of Strandburg *et al* [19] and Widom *et al* [18] deserves discussion. Strandburg

† We indulge in a little numerology and note the intriguing coincidence between the estimated value of  $S^0/n_{\text{tile}}^0$  and  $\ln \tau$ .

*et al* determined the stiffness constants by measuring the phason fluctuations of a Monte Carlo simulation. This is more direct than our approach where the stiffness constants are extracted by fitting the data to equation (39). Fitting for the stiffness constants, which are the coefficients of quadratic terms in  $\psi$  and  $w^\perp/w^\parallel$ , is difficult for noisy data because in effect it requires performing two numerical differentiations.

In [18] an entropy estimate was obtained for the constrained binary tiling with an accuracy comparable to that found here, but a much more accurate determination of the stiffness constant  $K = \frac{1}{2}(K_+ + K_-)$  was made. They calculated the entropy using the transfer-matrix for a series of small systems whose transverse boundary conditions minimized the phason strain. The curvature of the entropy function for these small systems was determined from the response of the entropy to varying a chemical potential. The results were extrapolated to the infinite size limit. The unexpectedly small region about  $E = 0$  to which equation (39) applies makes the fit for the stiffness constants, which is in effect equivalent to numerical differentiation, difficult given the accuracy of the TMCMC data. It may be more fruitful to follow [18] and calculate the second derivatives with respect to  $\psi_{yy}$  and  $\psi_{zy}$  for a similar set of small systems (in particular the  $\{F_n, F_n, F_{n-1}, F_{n-1}\}$  systems, where  $F_n$  is the  $n$ th Fibonacci number), and then extrapolate to the infinite size limit. Although this may allow accurate determination of  $(K_+ + K_-)$  and  $K_z$  (see equation (40)),  $(K_+ - K_-)$  could not be estimated by this technique.

In conclusion, we have described a way to implement a TMCMC computation of the entropy of a random Penrose tiling near zero phason strain. We have determined estimates of the maximum entropy density  $S^0$  and the stiffness constants  $K_+$ ,  $K_-$  and  $K_z$ . We have compared the efficacy of this computation to related Monte Carlo and finite-size transfer-matrix computations. We present for the first time an estimate of  $S^0$ , and independent estimates of  $K_+$  and  $K_-$ , for the random Penrose tiling.

## Acknowledgments

LJS was supported by the National Science Foundation through the Cornell Material Science Center, and CLH was supported by the US Department of Energy grant DE-FG02-89ER45405; the computation was done in part with the support of the Cornell National Supercomputing Facility. We are grateful for many helpful discussions to M Peter Nightingale, Michael Widom, and especially Veit Elser, who also provided detailed comments on the manuscript.

*Note added.* A more thorough discussion of thermodynamics including the use of chemical potentials, and some parallel discussion of the technicalities of transfer matrices, are in a very recent work on the phase diagram of the random eight-fold rhombus tiling [27].

## Appendix A. The transfer-matrix Monte Carlo method

### A.1. Basic theory

The transfer-matrix Monte Carlo (TMCMC) method [28] is a stochastic technique for doing matrix multiplications without storing the matrices or even the vectors. This makes TMCMC useful for calculations involving extremely large matrices. Here we will describe the algorithm for calculating the leading eigenvalue of a matrix with non-negative entries.



In the transfer-matrix Monte Carlo method [28] a population of  $M$  walkers labelled with the integers  $\{\alpha_1, \alpha_2, \dots, \alpha_M\}$  and the positive real numbers  $\{w_1, w_2, \dots, w_M\}$  represents the  $n$ -component vector

$$\mathbf{v} = \sum_{i=1}^M w_i \mathbf{e}_{\alpha_i} \quad (49)$$

where  $\mathbf{e}_k$  is the unit vector with a single non-zero entry in the  $k$ th position, and  $1 \leq \alpha_i \leq n$ . The  $\alpha$ 's and  $w$ 's are said to represent the 'positions' and 'weights' of the walkers respectively.

TMMC multiplication of  $\mathbf{v}$  by the transfer-matrix  $T$  is accomplished by performing a 'TMMC decomposition' of  $T$  into the product of a diagonal matrix  $D$  and a stochastic matrix  $P$ , i.e.  $T = PD$ , where, by definition, the sum of the entries in each column of a stochastic matrix is unity. Assume that all the entries of  $T$  are positive, then all the entries of  $P$  and  $D$  can also be positive, and the entries of  $P$  may be interpreted as probabilities. Upon the operation of  $P$  on the population representing  $\mathbf{v}$ , the position  $\alpha_i$  of each walker has the probability  $P_{\alpha'_i, \alpha_i}$  of changing to  $\alpha'_i$ . The weights are unchanged by  $P$ . On average, the vector equivalent (as in equation (49)) of the resulting population is equal to  $P\mathbf{v}$ . As  $M \rightarrow \infty$ , the vector equivalent of the TMMC operation of  $P$  on  $\mathbf{v}$  becomes equal to the matrix multiplication  $P\mathbf{v}$ . The matrix  $D$  operates on  $\mathbf{v}$  by changing the weights  $\{w_1, w_2, \dots, w_M\}$  of  $\mathbf{v}$  to  $\{D_{\alpha_1, \alpha_1} w_1, D_{\alpha_2, \alpha_2} w_2, \dots, D_{\alpha_M, \alpha_M} w_M\}$ , while leaving the positions unchanged. Clearly the vector equivalent of the TMMC operation of  $D$  on  $\mathbf{v}$  is equal to  $D\mathbf{v}$ . If the weights of the population representing  $\mathbf{v}$  are non-negative, the weights of  $T^m \mathbf{v}$  are also non-negative.

On repeated application of  $P$  and  $D$  to the population, some walkers will accrue very large weights and others will accrue very small weights. It is computationally advantageous to divide each of the walkers with larger weights into a number of walkers with smaller weights, and to conglomerate or annihilate walkers with very small weights. There are many algorithms for redistributing the positions and weights of the walkers while, on average, keeping the vector equivalent unchanged [28, 29]. We have found the following algorithm to reduce the variance of TMMC calculations and to be computationally efficient. Before redistribution, the population weight

$$W = \sum_j w_j / M_{\text{target}} \quad (50)$$

is factored from each walker weight  $w_i$  i.e.

$$w_i \rightarrow w_i / W = \frac{w_i M_{\text{target}}}{\sum_j w_j} \quad (51)$$

The population weight is to be considered as a scalar prefactor to the vector equivalent of the population. If the new scaled weight of a walker satisfies the bounds  $\frac{1}{2} \leq w_i < 2$ , the weight and position are left unchanged by redistribution. If  $2 \leq w_i$ , the walker at  $\alpha_i$  is replaced by  $[w_i]$  walkers at  $\alpha_i$ , each with a weight of  $w_i / [w_i]$ , where  $[x]$  is the greatest integer less than or equal to  $x$ . If  $w_i < \frac{1}{2}$ , the walker is replaced with a walker at the same position with a weight of unity with a probability  $w_i$ , and destroyed with a probability of  $1 - w_i$ . This algorithm insures that (i) the walker weights stay between  $\frac{1}{2}$  and 2, (ii) the number of walkers remains near  $M_{\text{target}}$ , and (iii) on average the vector equivalent of the population is unchanged.

The scalar prefactor of the vector equivalent of the population after  $\tau_\pi$  successive applications of the transfer-matrix and redistributions of the population, is the product

of the population weights  $W_1 W_2 \dots W_{\tau_\pi}$ . When using TMMC, the natural norm of an  $n$ -dimensional vector is the 1-norm:  $\|\mathbf{v}\|_1 = \sum_{i=1}^n |v_i|$ . After the  $\tau_\pi$ th scalar prefactor is divided from the population weights, but before the redistribution operation,

$$\|\mathbf{v}\|_1 = \left( \prod_{l=1}^{\tau_\pi} W_l \right) \sum_{j=1}^M w_j = \left( \prod_{l=1}^{\tau_\pi} W_l \right) M_{\text{target}}. \tag{52}$$

Estimation of the leading eigenvalue  $\lambda_0$  of  $\mathbf{T}$  utilizes the relation

$$\mathbf{v}_0 = \lim_{(\tau_\pi/\xi) \rightarrow \infty} \mathbf{T}^{\tau_\pi} \mathbf{v}_{\text{in}} \tag{53}$$

where the expansion of  $\mathbf{v}_{\text{in}}$  in terms of the eigenvectors of  $\mathbf{T}$  is required to contain a non-zero component of  $\mathbf{v}_0$ ,  $\lambda_0, \lambda_1, \lambda_2, \dots$  are the eigenvalues in order of descending magnitude,  $\xi^{-1} = \ln(\lambda_0/\lambda_1)$  is the correlation length, and  $\mathbf{v}_0 = (1/\lambda_0)\mathbf{T}\mathbf{v}$  is the leading eigenvector. The random Penrose tiling, as a critical system, has a correlation length on the order of the width of the system ( $\approx N_w$ ) [30].

The leading eigenvalue  $\lambda_0$  can be extracted either using the relationship

$$\lambda_0 = \lim_{\tau_\pi \rightarrow \infty} \frac{\|\mathbf{T}^{\tau_\pi+1} \mathbf{v}\|_1}{\|\mathbf{T}^{\tau_\pi} \mathbf{v}\|_1} \tag{54}$$

or

$$\lambda_0 = \lim_{\tau_\pi \rightarrow \infty} \left( \frac{\|\mathbf{T}^{\tau_\pi} \mathbf{v}\|_1}{\|\mathbf{v}\|_1} \right)^{1/\tau_\pi}. \tag{55}$$

In terms of the population weights, equations (54) and (55) lead to two alternative  $\lambda_0$  estimators:

$$\lambda_0^{(1)}(M, \tau_\sigma, \tau_\pi) = \frac{\sum_{i=1}^{\tau_\sigma} \prod_{j=1}^{\tau_\pi+1} W_{i+j}}{\sum_{i=1}^{\tau_\sigma} \prod_{j=1}^{\tau_\pi} W_{i+j}} \tag{56}$$

and

$$\lambda_0^{(2)}(M, \tau_\sigma, \tau_\pi) = \left( \frac{1}{\tau_\sigma} \sum_{i=1}^{\tau_\sigma} \prod_{j=1}^{\tau_\pi} W_{i+j} \right)^{1/\tau_\pi} \tag{57}$$

respectively. The  $\tau_\sigma$  summation performs an average over approximately  $\max\{\tau_\sigma/\xi, \tau_\sigma/\tau_\pi\}$  independent terms. The random fluctuations in the vector equivalent of the population with  $i+j$  insure that the vector equivalent of the population will generally contain a non-zero component of  $\mathbf{v}_0$  in an expansion in terms of the eigenvectors of  $\mathbf{T}$ . There are systematic and random errors associated with finite  $M$  and  $\tau_\sigma$ , but for  $\tau_\pi \gg \xi$  with  $M \rightarrow \infty$  or  $\tau_\sigma \rightarrow \infty$ ,  $\lambda_0^{(i)}(M, \tau_\sigma, \tau_\pi) \rightarrow \lambda_0$ .

### A.2. Implementation

Although the use of the estimator  $\lambda_0^{(2)}$  has been discouraged [31] because of the systematic error associated with finite  $\tau_\pi$ , from our experience this estimator is preferable to  $\lambda_0^{(1)}$ . The estimator  $\lambda_0^{(1)}$  has much more random error than  $\lambda_0^{(2)}$ , and the magnitude of the systematic error for the two estimators is about the same. Figure 4 shows  $\lambda_0^{(1)}$  and  $\lambda_0^{(2)}$  against  $\tau_\pi$  for a  $\{2, 1, 1, 1\}$  system with  $\mu_{52} = \mu_{34} = 0.0$ . Our calculations utilize  $\lambda_0^{(2)}$ , and for the remainder of the text we will simply refer to this estimator as *the* estimator.

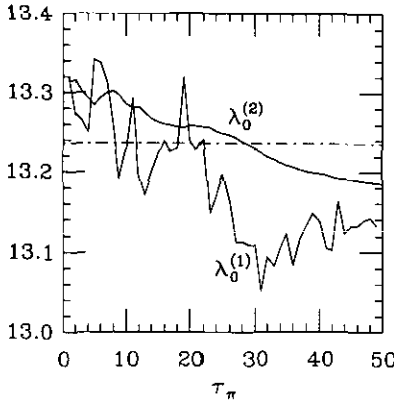


Figure 4. The estimators  $\lambda_0^{(1)}$  and  $\lambda_0^{(2)}$  from a single run for a  $\{2, 1, 1, 1\}$  system with  $\mu_{52} = \mu_{34} = 0.0$ ,  $M = 100$  and  $\tau_r = 100$ . The broken line marks the exact leading eigenvalue.

Calculation of  $\lambda_0$  requires the generation of  $\tau_\sigma + \tau_\pi - 1$  weights, and for large  $\tau_\sigma$  requires a computational effort that scales as  $N_W M \tau_\sigma$ . As figure 5 shows, the random and systematic errors are reduced as  $M/\tau_\sigma$  increases. For a given  $M$  and  $\tau_\sigma$ , the mean and standard deviation of  $\lambda_0(\tau_\pi)$  is calculated from an analysis of ten independent runs. The entropy estimate  $F_{\text{lay}}(M, \tau_\sigma)$  is obtained from

$$F_{\text{lay}}(M, \tau_\sigma) = \frac{1}{N_W} \sum_{\tau_\pi = N_W+1}^{2N_W} F_{\text{lay}}(M, \tau_\sigma, \tau_\pi) = \frac{1}{N_W} \sum_{\tau_\pi = N_W+1}^{2N_W} \ln \lambda_0(M, \tau_\sigma, \tau_\pi). \quad (58)$$

The estimated error for a  $F_{\text{lay}}$  computation is taken as the largest of several errors  $\mathcal{E}^{(1)}$ ,  $\mathcal{E}^{(2)}$  and  $\mathcal{E}^{(3)}$ , associated with the estimate.

The systematic error  $\mathcal{E}^{(1)}$  is estimated as the magnitude of the difference between the estimate  $F_{\text{lay}}(M, \tau_\sigma)$  and the estimate  $F_{\text{lay}}(M/2^{3/4}, \tau_\sigma/2^{1/4})$  requiring half the run time, i.e.

$$\mathcal{E}^{(1)} = \left| F_{\text{lay}}(M, \tau_\sigma) - F_{\text{lay}}\left(\frac{M}{2^{3/4}}, \frac{\tau_\sigma}{2^{1/4}}\right) \right| \quad (59)$$

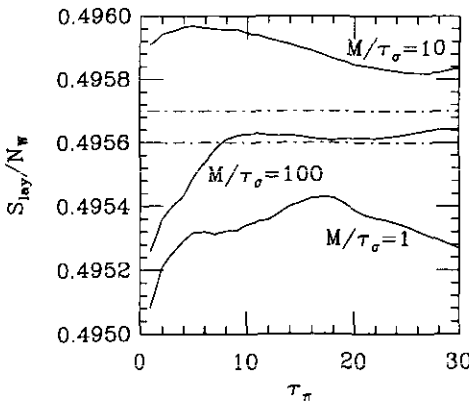


Figure 5. Estimates of  $F_{\text{lay}}/N_W$  from a single run for a  $\{4, 4, 2, 2\}$  system with  $\mu_{52} = -\mu_{34} = 0.4805$  for  $M/\tau_\sigma = 1, 10$  and  $100$  where  $M\tau_\sigma = 10^6$ . The broken lines bound the more accurate estimate  $F_{\text{lay}}/N_W = 0.49565$  (5). The random and systematic error decrease with increasing  $M/\tau_\sigma$ .

The random errors  $\mathcal{E}^{(2)}$  and  $\mathcal{E}^{(3)}$  are

$$\mathcal{E}^{(2)} = \max_{N_W \leq \tau_\sigma \leq 2N_W} |F_{\text{lay}}(M, \tau_\sigma) - F_{\text{lay}}(M, \tau_\sigma, \tau_\pi)| \quad (60)$$

and

$$\mathcal{E}^{(3)} = \max_{N_W \leq \tau_\pi \leq 2N_W} \delta F_{\text{lay}}(M, \tau_\sigma, \tau_\pi) \quad (61)$$

where  $\delta F_{\text{lay}}$  is the standard deviation of  $F_{\text{lay}}$ . For constant  $M\tau_\sigma$ ,  $\mathcal{E}^{(2)}$  and  $\mathcal{E}^{(3)}$  are relatively insensitive to  $N_W$ ; but  $\mathcal{E}^{(1)}$  grows rapidly (probably exponentially) with  $N_W$ . To obtain entropy estimates with an accuracy of about 0.1% or less we are restricted to system sizes  $N_W \leq 24$ . The errors  $\mathcal{E}^{(1)}$  and  $\mathcal{E}^{(3)}$  are typically of the same order of magnitude for those system sizes under consideration here.

To illustrate the typical parameters for a data point calculation we present two examples. The calculation of  $F_{\text{lay}}/N_W$  to an accuracy of 0.01% for the  $\{4, 4, 2, 2\}$  system with  $\mu_{52} = -\mu_{34} = 0.4805$  was achieved by a run with  $M = 20\,496$  and  $\tau_\sigma = 142$ , requiring 4.7 CPU hours on a Convex C210. The magnitudes of the errors were  $\mathcal{E}^{(1)} = 3.7 \times 10^{-5}$ ,  $\mathcal{E}^{(2)} = 2 \times 10^{-6}$  and  $\mathcal{E}^{(3)} = 4.9 \times 10^{-5}$ . For the  $\{6, 6, 3, 3\}$  system with  $\mu_{52} = -\mu_{34} = 0.4805$ , an accuracy of 0.06% was achieved by a run with  $M = 20\,489$  and  $\tau_\sigma = 142$  requiring seven CPU hours on the Convex. The magnitudes of the errors were  $\mathcal{E}^{(1)} = 3.1 \times 10^{-4}$ ,  $\mathcal{E}^{(2)} = 2 \times 10^{-6}$  and  $\mathcal{E}^{(3)} = 6.2 \times 10^{-5}$ .

## Appendix B. TMMC for the random Penrose tiling and importance sampling

### B.1. TMMC implementation of the tiling rules

The tiling rules and the TMMC method have been described in section 2.4 and appendix A, respectively. This section outlines the algorithm for a TMMC implementation of the tiling rules to compute the entropy of the tiling.

The entropy is computed by monitoring the population weight while repeatedly applying the transfer-matrix  $T = T_{SS}T_{SL}T_{LL}$  to the walkers. The diagonal operators of the TMMC decompositions of  $T_{SS}$ ,  $T_{SL}$  and  $T_{LL}$ , modify the weights of the walkers. The stochastic operators change the positions of the walkers, the position of a walker corresponding to a configuration of steps across a layer of the tiling.

The population weight is monitored after each application of the  $SS$  rule in the course of redistributing the walkers as described in appendix A. We have found that the point within the  $SS$ - $SL$ - $LL$  cycle at which the redistribution is implemented has little effect on the statistics of the estimate.

The  $T_{SS}$ ,  $T_{SL}$  and  $T_{LL}$  algorithms described in sections B.1.1-B.1.3 (i) perform the  $D$  operation by determining the sum of the weights of all possible step permutations consistent with the tiling rules and, increasing the walker weight by this factor, (ii) perform the  $P$  operation by stochastically choosing a new step configuration with a probability proportional to the weight of that configuration.

**B.1.1. The  $T_{SS}$  operation.** The string of steps is searched for all adjacent  $S^+S^-$  pairs (with the  $S^+$  on the left). Since the tiling has periodic boundary conditions, the sequence of steps across a layer is to be considered as periodic also. Each  $S^+S^-$  pair is a ' $T_{SS}$  operation interval.' For each  $S^+S^-$  pair the walker weight is increased by a factor of  $(1 + z_{34})$ , where  $z_{34} = e^{-\mu_{34}}$ . Each  $S^+S^-$  pair is switched to a  $S^-S^+$  pair with probability

$z_{34}/(1+z_{34})$ , and left unchanged with a probability  $1/(1+z_{34})$ . The  $T_{SS}$  operations for each  $T_{SS}$  operation interval are independent i.e.  $P_{SS}$  and  $D_{SS}$  may be decomposed into a direct product of matrices acting on individual  $S^+S^-$  pairs.

**B.1.2. The  $T_{SL}$  operation.** The string of steps is divided into ' $T_{SL}$  operation intervals'. The left-hand end of each operation interval starts with an  $S^+$  or immediately to the right of an  $S^-$ ; the right-hand end of each interval ends with an  $S^-$  or immediately to the left of an  $S^+$ . The interior of the interval consists entirely of  $L$  steps. For example, the layer of steps  $\{L^+L^-S^+L^+L^+S^+L^-S^-L^+L^-S^-\}$  consists of the  $T_{SL}$  operation intervals  $[S^+L^+L^+]$ ,  $[S^+L^-S^-]$ ,  $[L^+L^-S^-]$ , and  $[L^+L^-]$ . The  $T_{SL}$  operations for each  $SL$  interval are independent i.e.  $P_{SL}$  and  $D_{SL}$  may be decomposed into a direct product of matrices acting on individual  $SL$  intervals. The application of the  $SL$  rules to the four different types of  $T_{SL}$  operation intervals are as follows:

(i) The interval  $[S^+L_1L_2\dots L_{n-1}L_n]$  becomes  $[L_1L_2\dots L_{i-1}S^+L_i\dots L_{n-1}L_n]$ , where  $0 \leq i \leq n$ , with probability  $1/(n+1)$ . The weight is increased by a factor of  $(n+1)$ .

(ii) The interval  $[L_1L_2\dots L_{n-1}L_nS^-]$  becomes  $[L_1L_2\dots L_iS^-L_{i+1}\dots L_{n-1}L_n]$ , where  $0 \leq i \leq n$ , with probability  $1/(n+1)$ . The weight is increased by a factor of  $(n+1)$ .

(iii) The interval  $[S^+L_1L_2\dots L_nS^-]$  becomes  $[L_1\dots L_iS^+L_{i+1}\dots L_jS^-L_{j+1}\dots L_n]$ , where  $0 \leq i \leq j \leq n$ , with probability  $2/[(n+1)(n+2)]$ . The weight is increased by a factor of  $(n+1)(n+2)/2$ .

(iv) The interval  $[L_1L_2\dots L_{n-1}L_n]$  and the weight remain unchanged.

**B.1.3. The  $T_{LL}$  operation.** Strings of consecutive  $L$  steps are the ' $T_{LL}$  operation intervals'. The  $T_{LL}$  operations for each operation interval are independent, i.e.  $P_{LL}$  and  $D_{LL}$  may be decomposed into a direct product of matrices acting on individual  $T_{LL}$  operation intervals.

Computation of the stochastic and diagonal matrix entries for the  $LL$  rule is more difficult than for the  $SL$  and  $SS$  rules; the  $L$  strings can be of any length (as is the case for  $SL$  strings) and since there is a chemical potential attached to the  $(5, 2)$  tiles, different permutations of the original string have different weights (as is the case with the  $SS$  rule). We introduce a diagrammatic method for performing the  $T_{LL}$  operations. Each initial configuration of  $L$  steps corresponds to a different diagram [14] on the square lattice (see figure 6; compare figure 5 of [14]). To optimize the computation speed, diagrams for all  $L$  strings up to length eight are stored in a look-up table. In the unlikely event that a longer  $L$  string occurs, the diagram is generated and used, but not stored.

A sequence of  $L$  steps corresponds to a path on the diagram, the  $L^+$  and  $L^-$  steps corresponding to  $(0, 1)$  and  $(1, 0)$  displacements, respectively. (This is simply a rotation and distortion of the actual sequence of steps.) Each  $LL$  exchange operation conserves the number of  $L^+$  and  $L^-$  steps in a string, while moving a segment of the path up and to the left. Therefore any allowed  $LL$  permutation of an initial string produces a path which lies above and to the left of the initial path, yet begins and ends at the same points as the initial path. The initial sequence of  $L$ 's is mapped to a path on the square lattice starting at the origin and ending at  $(x', y')$  (see the full curve in figure 6). The 'partial weight' at an intermediate point  $(x, y)$  along an allowed permutation of steps is defined as  $e^{-m\mu_{52}} = z^m$  (the subscript on the  $z$  has been dropped for notation convenience) where  $m$  is the number of whole or half  $(5, 2)$  tiles between the allowed permutation path and the initial path from point  $(x, y)$  to the left-hand end. Each lattice point  $(x, y)$  on the diagram is labelled with the sum  $w(x, y)$  of the partial weights

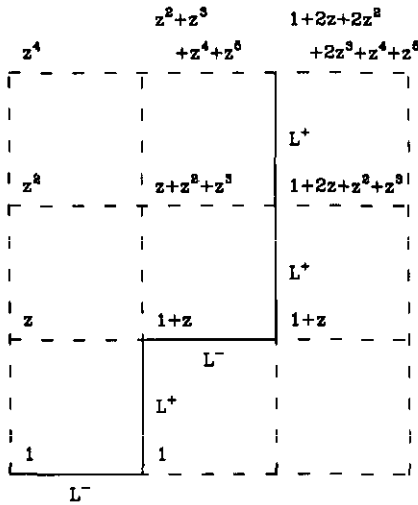


**Figure 6.**  $T_{LL}$  diagram for the sequence  $[L^- L^+ L^- L^+ L^+]$ . The values of  $w(x, y)$  are shown at lattice points.

of all allowed permutations by the following algorithm: (i) The origin is assigned a weight of unity. (ii) Lattice points below and to the right of the initial path have a weight of zero. (iii) For  $0 \leq y \leq y'$  and  $0 \leq x \leq x'$ ,  $w(x, y)$  is determined by

$$w(x, y) = f(x, y)(w(x - 1, y) + w(x, y - 1)) \tag{62}$$

where  $f(x, y) = z^{m(x,y)}$ . Here  $m(x, y)$  is the integer such that  $(x, y) + m(x, y)(1, -1)$  is a lattice point on the initial path (i.e., the number of steps across unit square diagonals to the initial path).

The weight of the walker is increased by a factor of  $w(x', y')$ , the sum of the weights of all allowed permutations. An allowed permutation of the initial sequence is chosen with a probability proportional to the weight of the permutation by stochastically tracing a path from  $(x', y')$  to the origin. A horizontal step from  $w(x, y)$  to  $w(x - 1, y)$  is taken with probability  $w(x - 1, y) / [w(x - 1, y) + w(x, y - 1)]$ , and a vertical step from  $w(x, y)$  to  $w(x, y - 1)$  is taken with probability  $w(x, y - 1) / [w(x - 1, y) + w(x, y - 1)]$ . The stochastic path is mapped to a string of  $L$ 's; again each  $L^+$  in the string (from left to right) corresponds to a displacement of  $(0, 1)$ , and each  $L^-$  corresponds to a  $(1, 0)$  displacement.

The average length of the  $T_{LL}$  and  $T_{SL}$  operation intervals, and the number of each type of operation interval per unit length, reach well-defined limits as the number of steps  $N_w$  across a layer becomes large. Since the TMMC operations may be decomposed into independent operations on the finite length operation intervals, the computation time per walker scales linearly with  $N_w$ . (In contrast, the computation time required to perform an exact transfer-matrix multiplication goes exponentially with  $N_w$ .)

### B.2. Importance sampling

Although importance sampling [32] was not implemented in the computation described in section 2, we outline the technique and present some conclusions concerning useful importance sampling transformations.

By the weighting algorithms outlined in this appendix, and equations (50) and (57), the variance of TMMC estimates vanishes when each of the diagonal matrices  $D_{SS}$ ,  $D_{SL}$  and  $D_{LL}$ , is proportional to the identity matrix. An effective importance sampling implementation performs a transformation on the transfer-matrices which makes the diagonal matrices more nearly proportional to the identity matrix, thereby reducing the variance of the estimates, while leaving the eigenvalue spectrum unchanged.

For simplicity we consider a transfer-matrix  $T = T_1 T_2$  ( $T_1$  and  $T_2$  are arbitrary), where  $u_1$  and  $u_2$  are the leading left eigenvectors of  $T_1 T_2$  and  $T_2 T_1$  respectively, i.e.

$$u_1 T_1 T_2 = \lambda_0 u_1 \quad \text{and} \quad u_2 T_2 T_1 = \lambda_0 u_2. \tag{63}$$

Then  $u_1 T_1 = u_2$ ,  $u_2 T_2 = u_1$ , and

$$1 U_1 T_1 U_2^{-1} = u_1 T_1 U_2^{-1} = \lambda_0 u_2 U_2^{-1} = \lambda_0 1 \tag{64}$$

$$1 U_2 T_2 U_1^{-1} = u_2 T_2 U_1^{-1} = \lambda_0 u_1 U_1^{-1} = \lambda_0 1 \tag{65}$$

where entries of the vector  $1$  are all unity, and  $U_i = \text{diag}(u_i)$ . The vector  $1$  is the leading left eigenvector of  $T_2^* = U_2 T_2 U_1^{-1}$  and  $T_1^* = U_1 T_1 U_2^{-1}$ , and therefore the diagonal parts of the TMMC decompositions of  $T_2^*$  and  $T_1^*$  are proportional to the identity matrix. Since  $T_1 T_2$  is related to

$$T_1^* T_2^* = (U_1 T_1 U_2^{-1})(U_2 T_2 U_1^{-1}) \tag{66}$$

by a similarity transformation, the eigenvalues of both products are the same. Matrices of the form  $VT_1 W^{-1}$  and  $VT_2 W^{-1}$ , where  $V$  and  $W$  are any diagonal matrices, are said to be the importance sampled versions of  $T_1$  and  $T_2$ .

Unfortunately, if we are using TMMC to determine the leading eigenvalue, the leading left eigenvectors are certainly not known. Effective importance sampling relies on finding vectors which (i) are a good approximation to the leading left eigenvectors, and (ii) are of a form such that the speed of the TMMC operations is not greatly reduced.

It is crucial that the importance sampling transformed matrices may be decomposed into direct products. Otherwise the advantages mentioned at the end of section B.1 are lost since a stochastic operation consists of a single random choice among all possible tiling permutations (a daunting prospect considering that the number of permutations grows exponentially with the system width while the weighting of each permutation is non-trivial).

Consider the TMMC application of some importance sampled matrix  $T^*$ ,

$$T^* = VTW^{-1} = P^* D^{**} W^{-1} = P^* D^* \tag{67}$$

where  $V$  and  $W$  are any two diagonal matrices, and  $P^* D^*$  and  $P^* D^{**}$  are the TMMC decompositions of  $T^*$  and  $VT$ , respectively. Useful forms of  $W^{-1}$  do not have to have the same operation intervals as  $D^{**}$  if we choose to apply  $W^{-1}$  and  $D^{**}$  sequentially. (Sequential application of these operations is equivalent to the application of their product since the matrices are diagonal and TMMC algorithm does not involve any random choices.) On the other hand, application of  $VT$  is not equivalent to sequential application of the two TMMC operations since the stochastic matrices of the TMMC decompositions of  $T$  and  $VT$  are different. For  $VT$  to maintain the same operation intervals as  $T$ , (i) the functional form of the entry  $V_{ii}$  must be a product of  $n$  factors, where  $n$  is the number of  $T$  operation intervals in the  $i$ th configuration, and (ii) only a single factor in the product must change on application of the  $T$  operations to a single operation interval. It is not clear whether there are useful importance sampling transformations for the tiling which satisfy the above restrictions.

### Appendix C. Application of 60-degree rhombus tiling

The 60° rhombus tiling is a non-quasicrystalline analogue of the Penrose tiling with a one-dimensional 'phason' space. The 60° rhombus tiles have edge vectors

$$\mathbf{d}_\alpha = (-\sin(2\pi\alpha/3), \cos(2\pi\alpha/3))$$

and vertices of a tiling are specified by  $\sum_{\alpha=1}^3 n_\alpha \mathbf{d}_\alpha$ . When the tile densities for each type of tile are equal, the entropy per tile is [33]

$$\approx 0.323\ 066. \quad (68)$$

A distortion of the tiling plane maps a 60° rhombus tiling onto a special case of the Penrose tiling using only three out of the ten types of rhombi. The mapping

$$\mathbf{d}_1 \rightarrow \mathbf{e}_1^\parallel \quad \mathbf{d}_2 \rightarrow -\mathbf{e}_4^\parallel \quad \mathbf{d}_3 \rightarrow -\mathbf{e}_3^\parallel$$

transforms a 60° rhombus tiling to a tiling of the (1, 3), (1, 4) and (3, 4) Penrose tiles. When  $n_{13} = n_{14} = n_{34}$ , the average area per tile is  $\approx 0.7088$ ; dividing the entropy in (68) by this figure, the entropy per unit area is  $\approx 0.4558$ . Similarly, mapping

$$\mathbf{d}_1 \rightarrow \mathbf{e}_1^\parallel \quad \mathbf{d}_2 \rightarrow \mathbf{e}_2^\parallel \quad \mathbf{d}_3 \rightarrow \mathbf{e}_5^\parallel$$

produces a tiling of the (1, 2), (1, 5) and (2, 5) Penrose tiles. When  $n_{12} = n_{15} = n_{25}$ , the average area per tile is  $\approx 0.8300$ , and the entropy per unit area is  $\approx 0.3893$ .

A comparison of the above exact values of the entropy density for special cases of the phason strain, with estimates produced using the results of section 4.1 and equation (16), confirms that there are significant corrections to the quadratic form assumed in equation (15). A random tiling of equal densities of (1, 3), (1, 4) and (3, 4) tiles has an entropy density of  $\approx 0.46$  and non-zero phason strain components  $E_{xx} = \tau$  and  $E_{yy} = \tau^{-2}$ . But, since  $K_+$  is at least as large as unity and the entropy density maximum  $S^0$  has a value of about 0.59, the entropy density according to equation (16) should be considerably negative (about  $-2$ ) with this phason strain. A similar analysis for the random tiling with equal densities of (1, 2), (1, 5) and (2, 5) tiles (non-zero phason strain components  $E_{xx} = \tau^{-1}$ ,  $E_{yy} = \tau^{-4}$  and  $E_{zy} = 2\sqrt{2}\tau^{-2}$ , and entropy density  $\approx 0.39$ ) shows that the entropy density according to equation (16) should again be negative ( $\approx -0.3$ ).

### References

- [1] Shechtman D S, Blech I, Gratias D and Cahn J W 1984 *Phys. Rev. Lett.* **53** 1951
- [2] Henley C L 1987 *Comment. Condens. Matter Phys.* **13** 59
- [3] Jarić M V (ed) 1988 *Aperiodicity and order, vol 1: Introduction to Quasicrystals* (Boston: Academic)
- [4] Jarić M V and Gratias D (ed) 1989 *Aperiodicity and order, vol 3: Extended Icosahedral Structures* (Boston: Academic)
- [5] Horn P M, Malzfeldt W, DiVincenzo D P, Toner J and Gambino R 1986 *Phys. Rev. Lett.* **57** 1444
- [6] Bancel P A, Heiney P A, Stephens P W, Goldman A I and Horn P M 1985 *Phys. Rev. Lett.* **54** 2422
- [7] Shechtman D S and Blech I 1985 *Metallurg. Trans. A* **16** 1005
- [8] Stephens P W and Goldman A I 1986 *Phys. Rev. Lett.* **56** 1168
- [9] Stephens P W 1989 *Aperiodicity and order, vol 3: Extended Icosahedral Structures* ed M V Jarić and D Gratias (Boston: Academic) pp 37-104
- [10] Elser V 1987 *Proc. XVth International Colloquium on Group Theory in Physics* ed R Gilmore and D H Feng (Singapore: World Scientific)



- [11] Elser V 1989 *Aperiodicity and order, vol 3: Extended Icosahedral Structures* ed V Jarić and D Gratias (Boston: Academic) pp 105–36
- [12] Levine D and Steinhardt P J 1984 *Phys. Rev. B* **53** 2477
- [13] Elser V 1985 *Phys. Rev. Lett.* **54** 1730
- [14] Henley C L 1988 *J. Phys. A: Math. Gen.* **21** 1649
- [15] Bancel P A 1989 *Phys. Rev. Lett.* **63** 2741
- [16] Henley C L 1990 *Quasicrystals and Incommensurate Structures in Condensed Matter* ed M J Yacamán, D Romeu, V Castaño and A Gómez (Singapore: World Scientific) p 152
- [17] Widom M 1990 *Quasicrystals* ed M V Jarić and S Lundqvist (Singapore: World Scientific)
- [18] Widom M, Deng D P and Henley C L 1989 *Phys. Rev. Lett.* **63** 310
- [19] Strandburg K J, Tang L-H and Jarić M V 1989 *Phys. Rev. Lett.* **63** 314
- [20] Tang L-H 1990 *Phys. Rev. Lett.* **64** 2390
- [21] Shaw L J, Elser V and Henley C L 1991 *Phys. Rev. B* **43** 3423
- [22] Kawamura H 1983 *Prog. Theor. Phys.* **70** 697
- [23] Bak P 1985 *Phys. Rev. B* **32** 5764
- [24] Lubensky T C 1988 *Aperiodicity and order, vol 1: Introduction to Quasicrystals* ed M V Jarić (Boston: Academic)
- [25] Gelfand M P and Fisher M E 1988 *Int. J. Thermophys.* **9** 713
- [26] Li W, Park H and Widom M 1990 *J. Phys. A: Math. Gen.* **23** L573
- [27] Li W, Widom M and Park H 1991 *J. Stat. Phys.* in press
- [28] Hetherington J H 1984 *Phys. Rev. A* **30** 2713
- [29] Nightingale M P 1988 *Proc. 3rd Int. Conf. Supercomputing I* (Boston, MA) ed L P Kartashev and S I Kartashev
- [30] Nightingale M P 1976 *Physica* **83A** 561
- [31] Nightingale M P and Blöte H W J 1986 *Phys. Rev. B* **33** 659
- [32] Nightingale M P 1990 *Finite-Size Scaling and Numerical Simulation of Statistical Systems* ed V Privman (Singapore: World Scientific) p 287  
Nightingale M P and Caffisch R G 1988 *Computer Simulation Studies in Condensed Matter Physics* ed D P Landau and H B Schüttler (Berlin: Springer)
- [33] Wannier G H 1950 *Phys. Rev.* **79** 357; 1973 *Phys. Rev. B* **7** 5017 (E)